



Assembling silicon quantum dots into wires, networks and rods via metal ion bridge

Journal:	<i>Nanoscale</i>
Manuscript ID	NR-ART-01-2018-000631.R2
Article Type:	Paper
Date Submitted by the Author:	11-Mar-2018
Complete List of Authors:	Ohata, Yuki; Kobe University Sugimoto, Hiroshi; Kobe University, Department of Electrical and Electronic Engineering Fujii, Minoru; Kobe University, Department of Electrical and Electronic Engineering, Graduate School of Engineering



Assembling silicon quantum dots into wires, networks and rods via metal ion bridge†

Yuki Ohata, Hiroshi Sugimoto* and Minoru Fujii*

Received 00th January 20xx,
Accepted 00th January 20xx

DOI: 10.1039/x0xx00000x

www.rsc.org/nanoscale

Wires and networks of Si quantum dots (QDs) with the length of over 1 μm and the width of ~ 30 nm are produced by bridging Si QDs by metal ions in a solution. It is shown that the width of the wires is almost independent of the preparation parameters and is always about 30 nm, except for the case when Si QDs larger than 30 nm are used, while the length of the wires depends strongly on the kinds of ions, the amount of ions and the amount of Si QDs in a solution. In addition to the microscopic size assemblies, macroscopic size rods of Si QDs with the width of ~ 20 μm are produced by using Zn^{2+} ions. The XPS analyses reveal that Si QDs are connected each other via a ZnO layer in the rod. The rods have much higher conductivity and photo-response than Si QD solids produced without metal ions.

Introduction

Colloidal semiconductor quantum dots (QDs) are versatile materials with unique electrical, optical, magnetic and thermoelectric properties due to the atomic-like discrete energy state structures and the large surface-to-volume ratio. Furthermore, assembling three-dimensional superstructures of QDs enables creation of new properties due to different inter-QDs interactions, such as the direct coupling of the energy states and the formation of mini-bands^{1–3}, the charge transfer via tunneling⁴ and the energy transfer^{5,6}. Several different techniques have been developed for the self-assembly of QDs. The simplest one is that using the Van der Waals interaction between QDs, which usually results in the formation of a close-packed structure^{7,8}. More active control of the superstructure is possible by using magnetic dipole and electric dipole interactions^{9–14}. Recently, programmed assembly of QDs into the crystal by using DNA-templated (-guided) processes have been reported^{15–18}. Coordination assembly of QDs via metal ions has also been intensively studied^{19,20}.

Among the processes for the formation of a QDs assembly, coordination assembly via metal ions has advantages in applications where efficient charge transfer between QDs is crucial. Nag *et al.*, studied the coordinate bonding of various kinds of metal ions on CdSe QDs and demonstrated that metal ions provide a convenient tool for tailoring optical, electronic, magnetic, and catalytic properties of QDs and the solids²¹. Hirai *et al.*, showed that coordination assembly of FeS_2 nanocrystals

via Zn^{2+} ions enhances charge transfer between nanocrystals and improves the photocatalytic activity¹⁹. It is plausible that similar process can be applied to a wider range of material systems and may overcome a common issue of QDs-based devices, *i.e.*, poor carrier mobility due to the hopping-like charge transport between QDs.

The purpose of this work is to develop a process to produce an assembly of Si QDs via metal ion bridges. Si QDs are a highly environmentally friendly nanomaterial and is considered to be a candidate for heavy metal free QDs in optoelectronics and biophotonics^{22,23}. The quality of Si QDs, especially the colloidal solution, has been improved rapidly for the past decade^{24–27} and very high quality colloidal solutions with the luminescence quantum yield exceeding 50% has been produced^{28–30}. The next step required to make Si QDs practically useful is the improvement of the conductivity of the assembly. Coordination assembly of Si QDs via metal ions can be a promising approach to overcome the problem, although there have been no attempts to bridge Si QDs via metal ions.

In this work, we develop a process for the growth of wires and networks of Si QDs from the colloidal solution by the coordination assembly via metal ions. We perform comprehensive studies to test many kinds of metal ions with different valence numbers and redox potentials. We also study the effects of the size and the surface property of Si QDs on the formation of the assemblies. We show that wires of Si QDs with the width of 25–35 nm and the length exceeding 1 μm can be grown in proper conditions. From the structural analyses combined with the chemical analyses, we will propose a model for the growth of Si QDs wires and networks. Finally, we produce a macroscopic size rod of Si QDs (width: ~ 20 μm) by mixing very large amounts of Si QDs and Zn^{2+} ions and study the current transport properties. We show that the conductivity is largely improved in the Si QDs rod compared to simple agglomerates of Si QDs made without metal ions.

*Department of Electrical and Electronic Engineering, Graduate School of Engineering, Kobe University, Rokkodai, Nada, Kobe 657-8501, Japan.
E-mail: Sugimoto@eedept.kobe-u.ac.jp

E-mail: fujii@eedept.kobe-u.ac.jp

†Electronic Supplementary Information (ESI) available: Optical transmittance spectra of Si QDs/ $\text{Zn}(\text{NO}_3)_2 \cdot 6\text{H}_2\text{O}$ mixed solutions, TEM images of Si QDs assemblies produced from different size Si QDs, PL intensity as a function of the number of metal ions, P 2p and B 1s XPS spectra, and I-V characteristic of a Si QDs solid produced without metal ions in dark and under irradiation. See DOI: 10.1039/x0xx00000x

Experimental

Preparation of Si QDs

For the metal-ion-induced assembly of Si QDs, we use a colloidal solution of B and P codoped Si QDs developed in our group^{31–33}. The preparation procedure of the codoped Si QDs is described in detail in Ref.³². Briefly, a Si-rich borophosphosilicate glass (BPSG) film prepared by an rf co-sputtering method was annealed in a N₂ gas atmosphere for 30 min to grow codoped Si QDs in a BPSG matrix. The diameter of Si QDs (*D*) was changed from 3.9 nm to 57 nm by changing the growth temperature from 1100 to 1500°C^{34,35}. Si QDs were isolated from BPSG matrices by etching in a HF solution (46 wt. %) for 1 hour and were transferred to methanol. B and P codoped Si QDs are dispersible in water and alcohol without any organic functionalization processes due to the negative surface potential (zeta potential: -30 mV at pH 7)³⁶. When the growth temperature is relatively low, typically < 1300°C, almost all Si QDs are dispersed in methanol. On the other hand, when the growth temperature is higher, a part of them agglomerates³⁴. Precipitates in methanol were removed by centrifugation (8000 rpm, 3 min) and a supernatant liquid was stored in a vial. After the removal of precipitates, the liquids were very clear and no precipitates were observed for more than a year.

Characterization

Before describing the procedure for the formation of a metal-ion-induced Si QDs assembly, we briefly summarize the property of codoped Si QDs used in this work. Fig. 1(a) shows a photo of a methanol solution of Si QDs grown at 1200°C. The concentration of Si QDs (*C*_{Si}) is 500 µg/ml. The solution is very clear and scattering free. The optical transmittance of the solution in the transparent range is almost 100% (Fig. 1(b)). Fig. 1(c) shows a transmission electron microscope (TEM) (JEM-2100F, JEOL) image of a Si QD grown at 1200°C. For the TEM observation, a Si QD solution was dropped on a carbon-coated copper grid. The lattice fringe corresponds to {111} planes of Si crystal (0.314 nm). The diameter is about 7 nm. Fig. 1(d) shows the infrared (IR) absorption spectra of Si QDs stored in methanol for 2 hours, 2 days and 7 days. The peaks around 1080 and 2100 cm⁻¹ are Si-O-Si and Si-H stretching vibration modes, respectively. The Si-H mode is dominant just after the preparation and becomes weak during the storage in methanol. On the other hand, the Si-O-Si mode grows during the storage. The number ratio of Si-H and Si-O bonds (Si-H : Si-O) estimated by taking into account the oscillator strengths^{37,38} is 95:5, 85:15 and 65:35 for the samples 2 hours, 2 days and 7 days stored in methanol, respectively.

Synthesis of metal-ion-induced Si QDs assembly

The procedure for the formation of a metal-ion-induced Si QDs assembly is very simple. 390 µl of a methanol solution of Si QDs was first prepared. The concentration of Si QDs in the solution was changed from 10 µg/ml to 500 µg/ml. 10 µl of a methanol solution of metal nitrate (NaNO₃ (≥99%, Wako), KNO₃ (≥99%, Wako), Zn(NO₃)₂·6H₂O (≥99.9%, Wako), Ni(NO₃)₂·6H₂O (≥99.9%, Wako), Ca(NO₃)₂·4H₂O (≥99.9%, Wako), Mg(NO₃)₂·6H₂O (≥99.5%,

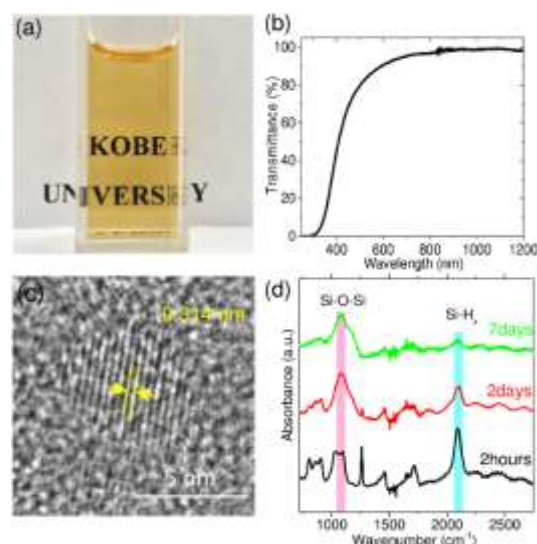


Fig. 1 (a) Photograph of methanol solution in which Si QDs are dispersed. (b) Optical transmittance spectrum of the solution in (a). (c) High-resolution TEM image of a Si QD. (d) IR absorption spectra of Si QDs stored in methanol for 2 hours, 2 days and 7 days.

Wako), Mn(NO₃)₂·6H₂O (≥99.5%, Wako), In(NO₃)₃·3H₂O (≥98%, Wako), and Al(NO₃)₃·9H₂O (≥99.9%, Wako)) was then prepared. The concentration was changed from 0.1 mM to 10 mM. These solutions were mixed and stirred for 30 minutes at room temperature by a magnetic stirrer. All the processes were performed in an ordinary laboratory environment.

Result and discussion

We prepare metal-ion-induced Si QDs assemblies by changing various parameters. First, we study the effect of the valence number of metal ions for the formation of an assembly. For this experiment, we fix the size of Si QDs to 7 nm and the concentration in methanol (*C*_{Si}) to 50 µg/ml. Fig. 2(a) shows the transmittance spectra of Si QDs/KNO₃ mixed solutions with different KNO₃ concentrations. The KNO₃ concentration is changed so that the number of K⁺ ions per a Si QD ([K⁺]/[Si QD]) becomes 50, 100 and 1000. The transmittance spectrum is not modified by the mixing (Fig. 2(a)) even when KNO₃ concentration is very high, suggesting that Si QDs assemblies are not formed. In fact, no agglomerates are observed in the TEM images in Fig. 2(b)–(d).

When a divalent metal nitrate (Zn(NO₃)₂·6H₂O) is mixed (Fig. 2(e)), the transmittance decreases in the short wavelength range at high [Zn²⁺]/[Si QD]. In the TEM images in Fig. 2(f) ([Zn²⁺]/[Si QD] = 50), we can recognize the formation of agglomerates of Si QDs. The agglomerates are not isotropic and are elongated in one direction. The average width (*d*_{ave}) of the agglomerates estimated from TEM images is about 30 nm and the average length (*l*_{ave}) is 78.8 nm with the standard deviation (σ) of 38.5 nm. The QDs wires become much longer in [Zn²⁺]/[Si QD] = 100 (*l*_{ave} = 418.0 nm (σ = 252.6 nm)) (Fig. 2(g)), although the width does not change so much. Further increase of [Zn²⁺]/[Si QD] results in the formation of the network of QDs

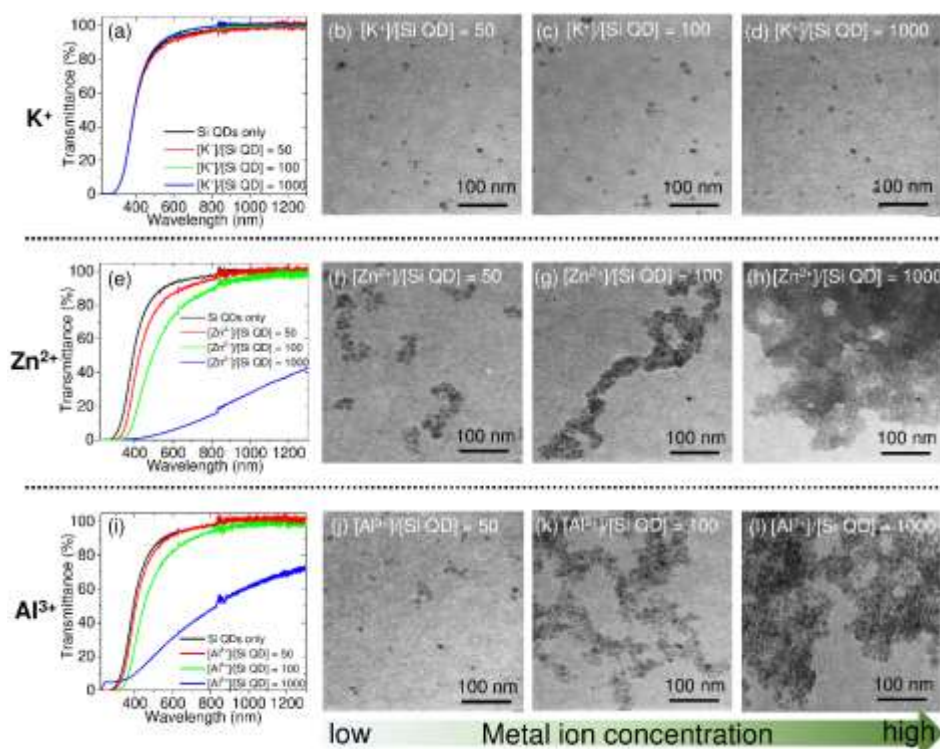


Fig. 2 (a, e, i) Optical transmittance spectra of solutions containing Si QDs 7 nm in diameter ($C_{Si} = 50 \mu\text{g/ml}$) and metal salts; (a) KNO_3 , (e) $\text{Zn}(\text{NO}_3)_2 \cdot 6\text{H}_2\text{O}$ and (i) $\text{Al}(\text{NO}_3)_3 \cdot 9\text{H}_2\text{O}$. The concentration of metal salts is changed so that the number ratio of metal ions to Si QDs ($[\text{Metal ions}]/[\text{Si QD}]$) becomes 0, 50, 100, 1000. (b-d, f-h, j-l) TEM images of Si QDs assemblies in the mixed solutions; (b-d) $[\text{K}^+]/[\text{Si QD}] = 50, 100, 1000$, (f-h) $[\text{Zn}^{2+}]/[\text{Si QD}] = 50, 100, 1000$, and (j-l) $[\text{Al}^{3+}]/[\text{Si QD}] = 50, 100, 1000$.

wires (Fig. 2(h)). Similar results are obtained in the case of trivalent metal nitrate ($\text{Al}(\text{NO}_3)_3 \cdot 9\text{H}_2\text{O}$) (Fig. 2(i-l)). The observed clear difference between the monovalent and multivalent ions for the formation of Si QDs wires is consistent with the Schulze-Hardy rule³⁹, which states that the critical coagulation concentration varies as the inverse sixth power of the counter ion charge. In negatively-charged Si QDs, multivalent metal cations represent highly effective coagulants. In the following, we will focus on divalent metal ions.

The critical coagulation concentration also depends on the type of ions, even if they carry the same charge. Fig. 3(a)-(c) shows TEM images of Si QDs assemblies produced by using different divalent metal ions, *i.e.*, Ca^{2+} , Mg^{2+} and Ni^{2+} . The Si concentration and the number ratio of metal ions and Si QDs ($[\text{Metal ions}]/[\text{Si QD}]$) are fixed to $50 \mu\text{g/ml}$ and 50, respectively. The average diameter of Si QDs is 7 nm. The size of agglomerates depends strongly on the kinds of ions. In Fig. 7(d), the length of QDs wires is plotted as a function of the standard redox potential of the divalent ions, Ca^{2+} (-2.84 V), Mg^{2+} (-2.35 V), Mn^{2+} (-1.18 V), Zn^{2+} (-0.762 V) and Ni^{2+} (-0.257 V). Longer wires are grown in metal ions with higher reduction potentials (smaller ionization tendency). This suggests that reduction of metal ions by Si QDs initiates the coagulation. When even higher redox potential metal ions such as Au^{3+} (1.52 V), Pt^{2+} (1.118 V), Ag^+ (0.7960 V) are mixed with Si QDs, they are reduced and precipitate on Si QDs⁴⁰. The absence of coagulation in Si QDs/ KNO_3 mixed solutions (Fig. 2(a-d)) is partly due to very small redox potential of K^+ (-2.925 V).

In addition to the reduction potential of metal ions, the property of the counter ion, *i.e.*, a Si QD, affects the critical coagulation concentration. As described above, the surface of Si QDs just after the preparation is H-terminated, and it is slowly oxidized during storage in methanol. Fig. 4(a)-(c) shows TEM images of Si QDs assemblies produced from Si QDs stored in methanol for 2 hours, 2 days and 7 days, respectively. Zn^{2+} is used as a metal cation. The Si QDs concentration and $[\text{Zn}^{2+}]/[\text{Si QD}]$

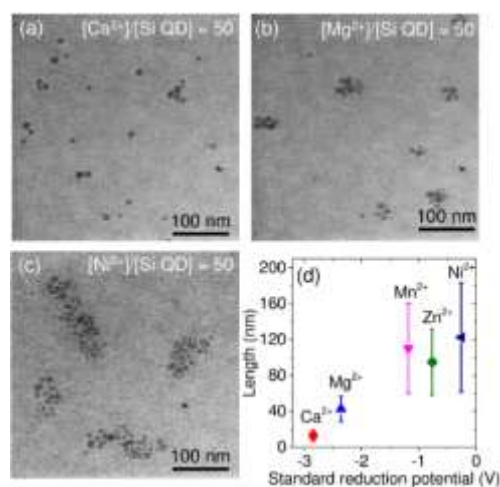


Fig. 3 TEM images of Si QDs assemblies in methanol solutions containing Si QDs 7 nm in diameter ($C_{Si} = 50 \mu\text{g/ml}$) and metal salts; (a) $\text{Ca}(\text{NO}_3)_2 \cdot 4\text{H}_2\text{O}$, (b) $\text{Mg}(\text{NO}_3)_2 \cdot 6\text{H}_2\text{O}$ and (c) $\text{Ni}(\text{NO}_3)_2 \cdot 6\text{H}_2\text{O}$. Length of Si QDs wires as a function of the standard reduction potential of metal ions.

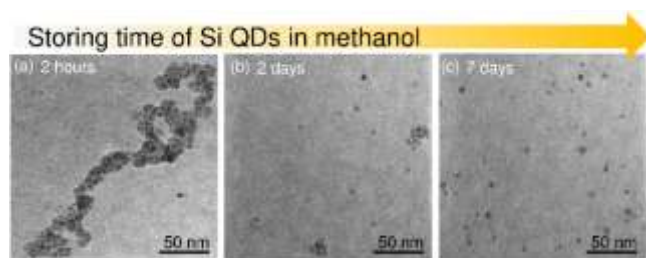


Fig. 4 TEM images of Si QDs assemblies in Si QDs/ $\text{Zn}(\text{NO}_3)_2 \cdot 6\text{H}_2\text{O}$ mixed solutions. Si QDs stored in methanol for (a) 2 hours, (b) 2 days and (c) 7 days are used for the reaction. Si QDs concentration and $[\text{Zn}^{2+}]/[\text{Si QD}]$ are fixed to $50 \mu\text{g/ml}$ and 100, respectively.

QD] are fixed to $50 \mu\text{g/ml}$ and 100, respectively. Si QDs wires are grown only when very fresh Si QDs are used. In Si QDs stored 2 days in methanol, only clusters of 8 to 9 Si QDs are formed. When the storage time is 7 days, no agglomerates are grown. The difference between Fig. 4(a)–(c) can also be seen in the optical transmittance spectra of the solutions (see Supporting Information, Fig. S1[†]). The result that the agglomeration proceeds efficiently only in fully H-terminated Si QDs suggests that a H-related chemical reaction is involved in the agglomeration process.

In order to study the mechanism of the anisotropic growth of Si QDs assembly, we performed TEM observations of the assemblies produced in smaller $[\text{metal ion}]/[\text{Si QD}]$ ranges than in Figs. 2–4. Fig. 5(a)–(d) shows the TEM images of Si QDs assemblies in Si QDs/ $\text{Ni}(\text{NO}_3)_2 \cdot 6\text{H}_2\text{O}$ mixed solutions. The concentration of Si QDs is fixed to $100 \mu\text{g/ml}$ and $[\text{Ni}^{2+}]/[\text{Si QD}]$ is 20, 30, 40 and 50. At the smallest $[\text{Ni}^{2+}]/[\text{Si QD}]$ (Fig. 5(a)), majority of Si QDs are isolated and clusters consisting of 5–8 Si QDs are observed. The shape of the clusters is almost isotropic. When $[\text{Ni}^{2+}]/[\text{Si QD}]$ is increased to 30 (Fig. 5(b)), isolated Si QDs disappear and the number of clusters increases. The size and shape of the clusters do not change significantly. Increase of

$[\text{Ni}^{2+}]/[\text{Si QD}]$ to 40 (Fig. 5(c)) initiates an anisotropic growth of the clusters. The width of the wires is almost the same as the size of clusters in Fig. 5(b). Further increase of $[\text{Ni}^{2+}]/[\text{Si QD}]$ (Fig. 5(d)) results in the elongation of the wires and the formation of a network structure, while the width of the wires is almost the same as that in Fig. 5(c). The length of Si QDs wires depends not only on $[\text{Ni}^{2+}]/[\text{Si QD}]$, but also on the amount of the ingredients. In Fig. 5(e), the Si ($200 \mu\text{g/ml}$) and Ni^{2+} concentration were doubled compared to the solution in Fig. 5(c) by keeping $[\text{Ni}^{2+}]/[\text{Si QD}]$ to 30. We can see extensive growth of Si QDs networks. Interestingly, the width of Si QDs wires is again 25–35 nm. Fig. 5(f) shows a high-resolution TEM image of a very thin part of a Si QDs wire. We can see that the wire is composed of Si QDs with high crystallinity. Fig. 5(g) and (h) shows a high-angle annular dark field (HAADF) scanning TEM (STEM) image and an energy-dispersive X-ray spectroscopy (EDS) element mapping image of Si, respectively. These images also confirm that the wires are composed of Si QDs. EDS signal of Ni was too small to be detected.

In order to know the origin of the magic number of the width of Si QDs wires, *i.e.*, 25–35 nm, we produce the assemblies by using different size Si QDs. Fig. 6(a)–(d) shows TEM images of Si QDs wires produced from 4, 7, 13 and 50 nm diameter Si QDs, respectively. Several TEM images in the same samples are shown in the Supporting Information (Fig. S2[†]). The relation between the width of the wires and the diameter of Si QDs is shown in Fig. 6(e). The width is almost independent of the Si QDs diameter, when it is in the range from 4 to 13 nm. As a result, the number of Si QDs in the thickness direction of a wire (right axis in Fig. 6(e)) decreases from 8 to 2. When the diameter of Si QDs exceeds 30 nm, a one-dimensional array of Si QDs is formed (Fig. 6(d)).

The data in Fig. 2–6 suggest the following process for the growth of Si QDs wires and networks. First, Si QDs assemblies 25–35 nm in diameter are grown in mixture solutions of Si QDs

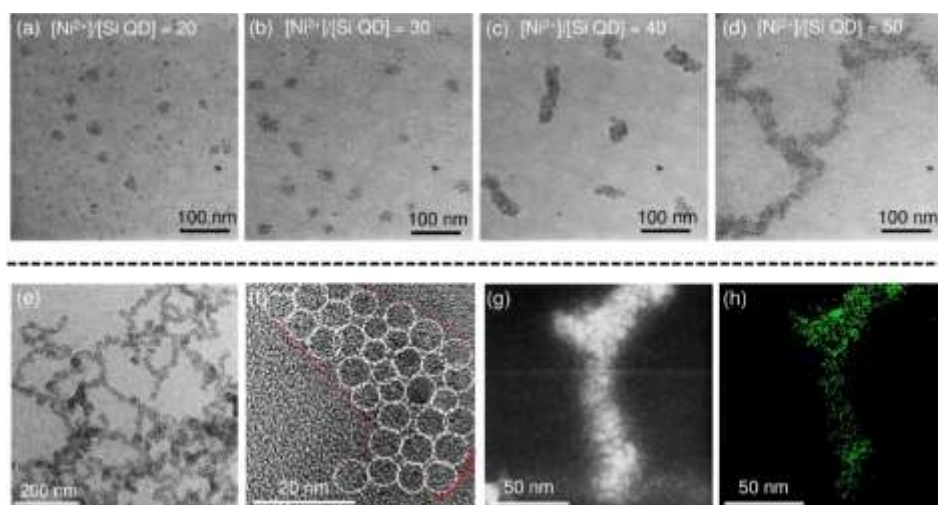


Fig. 5 (a–e) TEM images of Si QDs assemblies in Si QDs/ $\text{Ni}(\text{NO}_3)_2 \cdot 6\text{H}_2\text{O}$ mixed solutions; In (a–d), Si concentration is fixed to $100 \mu\text{g/ml}$ and $[\text{Ni}^{2+}]/[\text{Si QD}]$ is changed; (a) 20, (b) 30, (c) 40 and (d) 50. In (e), Si concentration is $200 \mu\text{g/ml}$ and $[\text{Ni}^{2+}]/[\text{Si QD}]$ is 30. (f) High-resolution TEM, (g) HAADF STEM and (h) STEM-EDS mapping (Si) images of a part of (e).

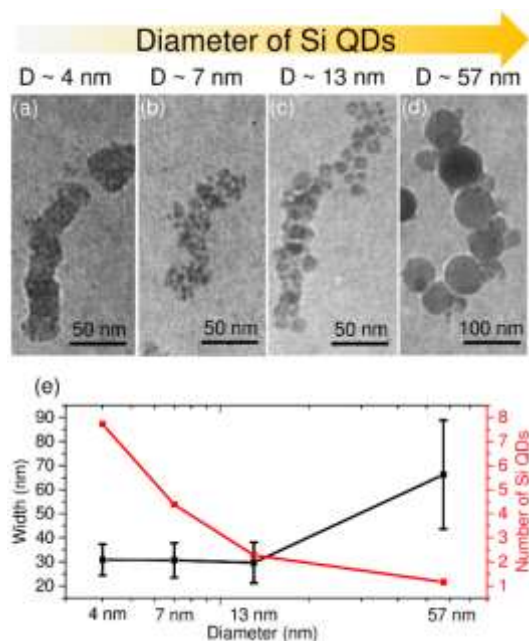


Fig. 6 TEM images of Si QDs assemblies produced by different size Si QDs. (a) $D = 4.0$ nm, $[\text{Ni}^{2+}]/[\text{Si QD}] = 100$, $C_{\text{Si}} = 10$ $\mu\text{g}/\text{ml}$, (b) $D = 7.0$ nm, $[\text{Ni}^{2+}]/[\text{Si QD}] = 30$, $C_{\text{Si}} = 100$ $\mu\text{g}/\text{ml}$, (c) $D = 13$ nm, $[\text{Zn}^{2+}]/[\text{Si QD}] = 100$, $C_{\text{Si}} = 10$ $\mu\text{g}/\text{ml}$, (d) $D = 57$ nm, $[\text{Zn}^{2+}]/[\text{Si QD}] = 50$, $C_{\text{Si}} = 10$ $\mu\text{g}/\text{ml}$. (e) Width of Si QDs wires as a function of the diameter of Si QDs. Right axis is the number of Si QDs in the thickness direction.

and metal salts, and then coalescence growth of the clusters starts if the amount of clusters exceeds a certain threshold. The initial isotropic growth of Si clusters is explained by the decrease of the surface potential of negatively charged Si QDs due to the adsorption of positively-charged metal ions and by the weakening of the Coulombic repulsion between Si QDs. In addition to this effect, adsorption of a positively-charged ion on the surface of a negatively-charged Si QD induces an anisotropy in the charge distribution in the Si QD, and the QD can be regarded as an electric dipole. The Coulombic attraction between the dipoles results in the formation of a one-dimensional array of Si QDs^{20,41–45}. In the present system, the former effect seems to be dominant until the size of the cluster becomes 25–35 nm. Above the size, the latter effect controls the agglomeration and one-dimensional wires and wire networks are grown by keeping the width to 25–35 nm. In addition to the Coulombic interaction, a chemical reaction plays a crucial role for the formation of agglomerates, because agglomeration proceeds efficiently only in fully H-terminated Si QDs as can be seen in Figure 4. It is plausible that the shape of the agglomerates is determined by the above mentioned process, and the formation of chemical bonds between Si QDs and metal ions is crucial to stabilize the agglomerates.

The process in the formation of agglomerates, *i.e.*, mixture of a Si QDs solution with that of metal ions, affects the luminescence property of Si QDs. In the condition that agglomerates are formed, the luminescence is severely quenched. On the other hand, in the condition that no agglomerates are formed, *e.g.*, mixture of a Si QDs solution with

that of monovalent metal ions, the quenching is much less serious (Figure S3† in Supporting Information).

We now turn our attention to much larger size Si QDs assemblies produced by much higher concentrations of Si QDs and metal ions for the measurements of the macroscopic properties. Fig. 7(a) and (b) shows optical microscope and scanning electron microscope, respectively, images of Si QDs assemblies produced by using Zn^{2+} ions. The Si concentration is 500 $\mu\text{g}/\text{ml}$ and $[\text{Zn}^{2+}]/[\text{Si QD}]$ is 10,000. We can see growth of rods with the width of about 20 μm and the length of about 100 μm . Interestingly, even in this extreme condition mixing very large amounts of Si QDs and metal salt, structural anisotropy of the shape is hold, although the width of the rod is much larger than that of the wires produced in milder conditions in Figs. 2–6.

In order to obtain information on the chemical bonds in the large assembly, we perform the XPS measurements (Al $\text{K}\alpha$ X-ray

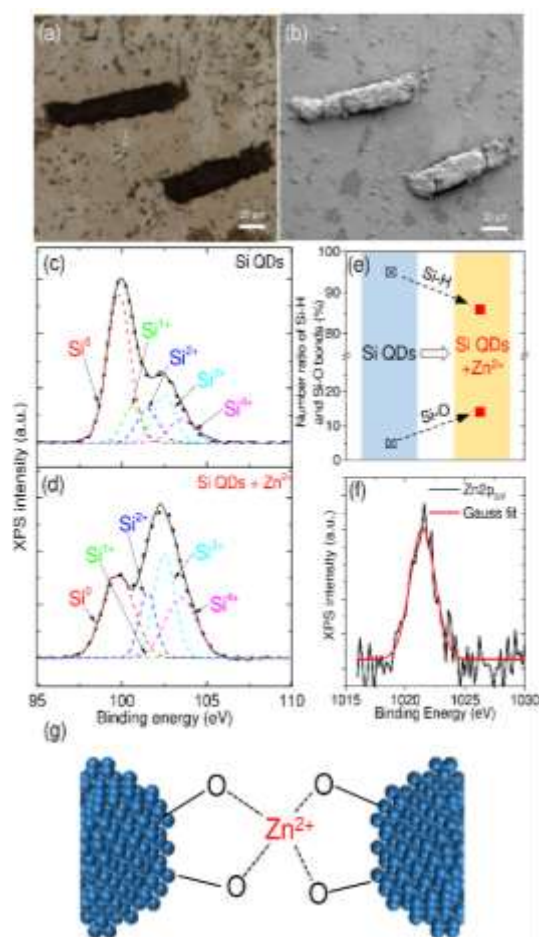


Fig. 7 (a) Optical microscope and (b) SEM images of Si QDs assemblies (rods) produced by mixing very large concentration solutions of Si QDs and Zn^{2+} ions; $C_{\text{Si}} = 500$ $\mu\text{g}/\text{ml}$ and $[\text{Zn}^{2+}]/[\text{Si QD}] = 10,000$. Si 2p XPS spectra of (c) Si QDs and (d) Si QDs assembly. (e) Number ratio of Si-O and Si-H bonds estimated from IR absorption spectra before and after the formation of Si QDs assembly. (f) Zn 2p_{3/2} XPS spectrum of Si QDs assembly. (g) Schematic illustration of the structure of Si QDs assembly.

source, PHI X-tool, ULVAC-PHI). Fig. 7(c) shows the Si 2p XPS spectrum of Si QDs (7 nm in diameter) stored in methanol for 2 hours. For the XPS measurements, a Si QDs solution was dropped on a gold-coated metal plate. Broken curves are the results of the decomposition of the peak into five Gaussian functions. Each curve corresponds to different valence states of Si, *i.e.*, Si⁰ (99.8 eV), Si¹⁺ (100.7 eV), Si²⁺ (101.5 eV), Si³⁺ (102.5 eV) and Si⁴⁺ (103.5 eV)^{46–49}. Before the formation of the assembly, Si⁰ is dominant⁵⁰. By the formation of the assembly (Fig. 7(d)), the intensity of the Si⁰ signal decreases, while those of Si²⁺ and Si³⁺ signals grow. Therefore, the formation of the assembly is accompanied by slight oxidation of Si QDs. This is consistent with the IR absorption data, which show the increase of the number of Si-O bonds and the decrease of that of Si-H bonds by the formation of the assembly (Fig. 7(e)). In the Supporting Information (Figure S4[†]), P 2p and B 1s XPS spectra of Si QDs and the assembly are shown. The P 2p peak around 130 eV and the B 1s one around 187–188 eV can be assigned to neutral (non-oxidized) P and B, respectively⁵¹. Since the spectra are not modified by the formation of Si QDs assembly, dopant sites are considered to be not directly related to the bridging sites. Fig. 7(f) shows the Zn 2p_{3/2} XPS spectrum. A peak at 1022.35 eV coincides with that of ZnO (1022.1 ± 0.4 eV), indicating that Zn atoms are attached on Si QD surface via an oxygen atom. By taking into accounts these results, the structure of a Si QDs assembly is considered to be that schematically shown in Fig. 7(g). Zn is attached on the surface of Si QDs via oxygen atoms and bridges Si QDs, *i.e.*, Si-O-Zn

bonds are formed on the surface Si QDs. In other word, Si QDs are connected each other via ZnO.

The number ratio of Si and Zn estimated from the XPS data in Fig. 7 is 67. From a rough estimation under the assumption that the escape depth of a photoelectron is 2 nm, this number corresponds to 121 Zn atoms per a Si QD. If a monolayer of ZnO is formed on the surface of a Si QD, about 6% of the surface is covered by ZnO.

In PbSe QDs, infilling the gap between QDs by ZnO improves the carrier mobility significantly due to the lowering of the height of the inter-QD tunneling barrier⁵². A similar effect can be expected in our Si QDs rods, although only a small region of Si QDs surface has bonds with ZnO. Therefore, we measured the current-voltage (I-V) characteristics of the Si QDs rods in Fig. 7. For the measurements of the I-V characteristics and the photo-response, a solution of Si QDs rods was dropped on Au (50 nm)/Ti (10 nm) electrodes with the gap of 10 μm. Fig. 8(a) shows the optical microscope and SEM images of the structure, in which a Si QDs rod is placed between the electrodes by chance. The black curve in Fig. 8(b) shows the I-V curve in vacuum (1.4 × 10⁻² mbar) in dark at room temperature. The I-V curve is non-linear as has been commonly observed in Si QDs assemblies⁵³. The conductivity is about 3.67 × 10⁻⁷ S/cm at 30 V. In Fig. 8(b), we observe a photo response under irradiation at 405 nm, indicating that the Si QDs rod holds the semiconductor character.

The conductivity of Si QDs rods are three orders of magnitude larger than those of Si QDs solids made on the same electrode without metal ions (Supporting Information, Fig. S5[†]). However, this comparison is not very fair due to very large difference of the geometry between the rods and flat solids of Si QDs. In order to do fairer comparison of the conductivity, we prepare large interdigitated electrodes (width: 20 μm, separation: 20 μm, overlap: 2 mm) and dropped the solutions of Si QDs and the rods containing the same number of Si QDs on the electrodes. Fig. 8(c) and (d) shows the I-V curves of Si QDs solid made without metal ions and Si QDs rods, respectively, in vacuum (1.4 × 10⁻² mbar) at room temperature. In the former case, the electrode is covered by a very uniform QDs film, while in the latter case, only a very small area of the electrodes is bridged by the rods as can be seen in the inset in Fig. 8(d). Despite very small current path in Si QDs rods in Fig. 8(d), the conductivity is largely improved compared to that of the Si QDs solids produced without Zn²⁺. This confirms that the ZnO bridge improves the conductivity between Si QDs greatly.

Conclusions

We have succeeded in producing wires and networks of Si QDs by using bridges of divalent and trivalent metal ions. We found that the width of the wires is almost independent of the preparation parameters and is always 25–35 nm, except for the case when Si QDs larger than 30 nm are used. On the other hand, the length of the wires and the size of the networks depend

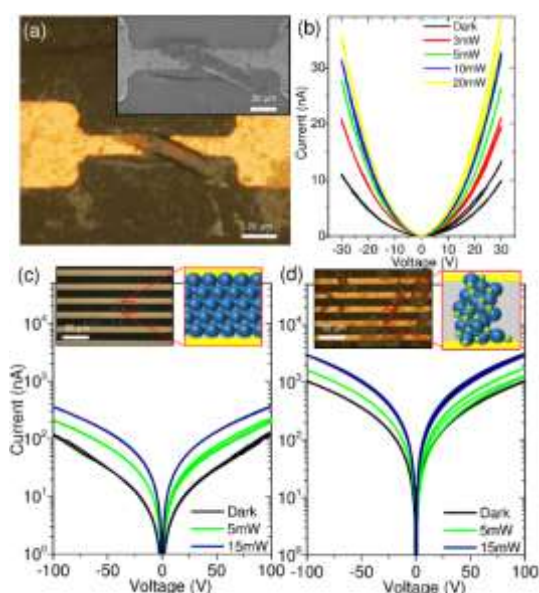


Fig. 8 (a) Optical microscope and SEM images of a Si QDs rod placed in between Au/Ti electrodes with the separation of 10 μm. (b) I-V characteristic of a Si QDs rod measured in vacuum at room temperature in dark and under light irradiation (λ = 405 nm). The irradiation power is changed from 3 to 20 mW. (c, d) I-V characteristic of (c) Si QDs solids produced without metal ions and (d) Si QDs rods on interdigitated electrodes measured in vacuum at room temperature in dark and under light irradiation (λ = 405 nm). The irradiation power is changed from 5 to 15 mW.

strongly on the kinds of ions, the amount of ions and the amount of Si QDs in a mixture solution. Furthermore, the surface property of Si QDs is a decisive factor for the formation of the assemblies. In proper conditions, the length of the wires exceeds 1 μm . In addition to the development of microscopic assemblies of Si QDs, we produced macroscopic size assemblies of Si QDs with the width of $\sim 20 \mu\text{m}$ by using Zn^{2+} ions. The XPS analyses revealed that Zn atoms are connected on Si QDs surface *via* O atoms and Si QDs are bridged by ZnO. In the Si QDs rods, the charge transport is significantly improved compared to that of Si QDs solids produced without metal ions. Therefore, assembling Si QDs *via* metal ion bridges is a promising approach to improve the performance of Si QDs-based optoelectronic devices.

Acknowledgements

This work was partly supported by the 2015 JST Visegrad Group (V4)–Japan Joint Research Project on Advanced Materials and JSPS KAKENHI Grant Number 16H03828.

Notes and references

- O. L. Lazarenkova and A. A. Balandin, *J. Appl. Phys.*, 2001, **89**, 5509–5515.
- A. Takahashi, T. Ueda, Y. Bessho, Y. Harada, T. Kita, E. Taguchi and H. Yasuda, *Phys. Rev. B*, 2013, **87**, 235323.
- J. Ravichandran, A. K. Yadav, R. Cheaito, P. B. Rossen, A. Soukiassian, S. J. Suresha, J. C. Duda, B. M. Foley, C. H. Lee, Y. Zhu, A. W. Lichtenberger, J. E. Moore, D. A. Muller, D. G. Schlom, P. E. Hopkins, A. Majumdar, R. Ramesh and M. A. Zurbuchen, *Nat. Mater.*, 2014, **13**, 168–172.
- M. M. Rahman, M. Igarashi, W. Hu, M. E. Syazwan, Y. Hoshi, N. Usami and S. Samukawa, in *2013 IEEE 39th Photovoltaic Specialists Conference (PVSC)*, IEEE, 2013, pp. 2456–2458.
- K. Furuta, M. Fujii, H. Sugimoto and K. Imakita, *J. Phys. Chem. Lett.*, 2015, **6**, 2761–2766.
- M. S. Kodaimati, C. Wang, C. Chapman, G. C. Schatz and E. A. Weiss, *ACS Nano*, 2017, **11**, 5041–5050.
- K. E. Mueggenburg, X. M. Lin, R. H. Goldsmith and H. M. Jaeger, *Nat. Mater.*, 2007, **6**, 656–660.
- M. G. Murray, C B; Kagan, C R; Bawendi, *Science (80-.)*, 1995, **270**, 1335.
- R. Mccartney, R. Buseck, B. Frankel, R. De Janeiro, R. De Janeiro and S. L. Obispo, *Eur. J. Mineral.*, 2001, **13**, 685–689.
- J. L. Kirschvink, M. M. Walker and C. E. Diebel, *Curr. Opin. Neurobiol.*, 2001, **11**, 462–467.
- B. Frankel, A. Bazylinski, R. Buseck, P. Street and S. L. Obispo, *Eur. J. Mineral.*, 2001, **13**, 671–684.
- D. V Talapin, E. V Shevchenko, C. B. Murray, A. V. Titov and P. Král, *Nano Lett.*, 2007, **7**, 1213–1219.
- T. Hanrath, D. Veldman, J. J. Choi, C. G. Christova, M. M. Wienk and R. A. J. Janssen, *ACS Appl. Mater. Interfaces*, 2009, **1**, 244–250.
- J. Yang, Y. Zhou, S. Zheng, X. Liu, X. Qiu, Z. Tang, R. Song, Y. He, C. W. Ahn and J. W. Kim, *Chem. Mater.*, 2009, **21**, 3177–3182.
- J. D. Le, Y. Pinto, N. C. Seeman, K. Musier-forsyth, T. A. Taton and R. A. Kiehl, *Nano Lett.*, 2004, **4**, 2434–2347.
- D. Nykypanchuk, M. M. Maye, D. van der Lelie and O. Gang, *Nature*, 2008, **451**, 549–552.
- H. Kuang, W. Ma, L. Xu, L. Wang and C. Xu, *Acc. Chem. Res.*, 2013, **46**, 2341–2354.
- D. Liu, S. L. Daubendiek, M. A. Zillman, K. Ryan, E. T. Kool, N. York and R. V August, *J. Am. Chem. Soc.*, 1996, **118**, 1587–1594.
- K. Hirai, B. Yeom, S. Chang, H. Chi, J. F. Mansfield, B. Lee, S. Lee, C. Uher and N. A. Kotov, *Angew. Chemie Int. Ed.*, 2015, **54**, 8966–8970.
- V. Sayevich, B. Cai, A. Benad, D. Haubold, L. Sonntag, N. Gaponik, V. Lesnyak and A. Eychmüller, *Angew. Chemie - Int. Ed.*, 2016, 1–6.
- A. Nag, D. S. Chung, D. S. Dolzhnikov, M. Nada, S. Chattopadhyay, T. Shibata and D. V Talapin, *J. Am. Chem. Soc.*, 2012, **134**, 13604–13615.
- T. Lin, X. Liu, B. Zhou, Z. Zhan, A. N. Cartwright and M. T. Swihart, *Adv. Funct. Mater.*, 2014, **24**, 6016–6022.
- Z. Ni, L. Ma, S. Du, Y. Xu, M. Yuan, H. Fang, Z. Wang, M. Xu, D. Li, J. Yang, W. Hu, X. Pi and D. Yang, *ACS Nano*, 2017, **11**, 9854–9862.
- M. Dasog, Z. Yang, S. Regli, T. M. Atkins, A. Faramus, M. P. Singh, E. Muthuswamy, S. M. Kauzlarich, R. D. Tilley and J. G. C. Veinot, *ACS Nano*, 2013, **7**, 2676–2685.
- C. M. Hessel, D. Reid, M. G. Panthani, M. R. Rasch, B. W. Goodfellow, J. Wei, H. Fujii, V. Akhavan and B. A. Korgel, *Chem. Mater.*, 2012, **24**, 393–401.
- M. L. Mastronardi, F. Maier-Flaig, D. Faulkner, E. J. Henderson, C. Kübel, U. Lemmer and G. A. Ozin, *Nano Lett.*, 2012, **12**, 337–342.
- L. Mangolini and U. Kortshagen, *Adv. Mater.*, 2007, **19**, 2513–2519.
- D. Jurbergs, E. Rogojina, L. Mangolini and U. Kortshagen, *Appl. Phys. Lett.*, 2006, **88**, 233116.
- F. Sangghaleh, I. Sychugov, Z. Yang, J. G. C. Veinot and J. Linnros, *ACS Nano*, 2015, **9**, 7097–7104.
- M. Greben, P. Khoroshyy, X. Liu, X. Pi and J. Valenta, *J. Appl. Phys.*, 2017, **122**, 34304.
- M. Fukuda, M. Fujii, H. Sugimoto, K. Imakita and S. Hayashi, *Opt. Lett.*, 2011, **36**, 4026–4028.
- H. Sugimoto, M. Fujii, K. Imakita, S. Hayashi and K. Akamatsu, *J. Phys. Chem. C*, 2012, **116**, 17969–17974.
- M. Fujii, H. Sugimoto and K. Imakita, *Nanotechnology*, 2016, **27**, 262001.
- H. Sugimoto, M. Fujii, K. Imakita, S. Hayashi and K. Akamatsu, *J. Phys. Chem. C*, 2013, **117**, 11850–11857.
- H. Sugimoto and M. Fujii, *Adv. Opt. Mater.*, 2017, **5**, 1700332.
- H. Sugimoto, M. Fujii, Y. Fukuda, K. Imakita and K. Akamatsu, *Nanoscale*, 2014, **6**, 122–6.
- and H. J. S. Suha Oguz, D. A. Anderson, William Paul, *Physical. Rev. B*, 1980, **22**, 880–885.
- S. Mukhopadhyay and S. Ray, *Appl. Surf. Sci.*, 2011, **257**, 9717–9723.
- H. L. ONG and R. E. BISQUE, *Soil Sci.*, 1968, **106**, 220–224.
- H. Sugimoto, M. Fujii and K. Imakita, *Nanoscale*, 2016.
- J. P. Pantina and E. M. Furst, *Langmuir*, 2006, **22**, 5282–5288.

- 42 J. Liao, Y. Zhang, W. Yu, L. Xu, C. Ge, J. Liu and N. Gu, *Colloids Surfaces A Physicochem. Eng. Asp.*, 2003, **223**, 177–183.
- 43 X. Han, J. Goebl, Z. Lu and Y. Yin, *Langmuir*, 2011, **27**, 5282–5289.
- 44 S. Si, M. Raula, T. K. Paira and T. K. Mandal, *ChemPhysChem*, 2008, **9**, 1578–1584.
- 45 A. N. Shipway, M. Lahav, R. Gabai and I. Willner, *Langmuir*, 2000, **16**, 8789–8795.
- 46 A. Barranco, F. Yubero, J. P. Espinos, J. P. Holgado and A. Caballero, *Vacuum*, 2002, **67**, 491–499.
- 47 T. Instruments, *Appl. Surf. Sci.*, 1993, **70–71**, 222–225.
- 48 W. L. Zhang, S. Zhang, M. Yang and T. P. Chen, *J. Phys. Chem. C*, 2010, **114**, 2414–2420.
- 49 Y. N. Sun, A. Feldman and E. N. Farabaugh, *Thin Solid Films*, 1988, **157**, 351–360.
- 50 M. Fujii, H. Sugimoto, M. Hasegawa and K. Imakita, *J. Appl. Phys.*, 2014, **115**, 84301.
- 51 J. Chastain, R. C. King and J. Moulder, *Handbook of X-ray photoelectron spectroscopy: a reference book of standard spectra for identification and interpretation of XPS data*, Physical Electronics Division, Perkin-Elmer Corporation Eden Prairie, Minnesota, 1992.
- 52 Y. Liu, M. Gibbs, C. L. Perkins, J. Tolentino, M. H. Zarghami, J. Bustamante and M. Law, *Nano Lett.*, 2011, **11**, 5349–5355.
- 53 S. Kano, M. Sasaki and M. Fujii, *J. Appl. Phys.*, 2016, **119**, 215304.